Journal of Computational Physics 323 (2016) 149–170

Contents lists available at ScienceDirect

Journal of Computational Physics

www.elsevier.com/locate/jcp

A mass-redistributed finite element method (MR-FEM) for acoustic problems using triangular mesh

Z.C. He [a,b,1], Eric Li [a,c,*,1], G.R. Liu [d], G.Y. Li [a,b,*], A.G. Cheng [a,b]

[a] State Key Laboratory of Advanced Design and Manufacturing for Vehicle Body, Hunan University, Changsha, 410082, PR China
[b] Joint Center for Intelligent New Energy Vehicle, Shanghai, 201804, PR China
[c] Department of Mechanical and Automation Engineering, The Chinese University of Hong Kong, Shatin, NT, Hong Kong, China
[d] School of Aerospace Systems, University of Cincinnati, Cincinnati, OH 45221-0070, USA

ARTICLE INFO

Article history:
Received 28 September 2015
Received in revised form 19 July 2016
Accepted 21 July 2016
Available online 27 July 2016

Keywords:
Acoustic
Numerical method
Mass-redistributed finite element method (MR-FEM)
Dispersion error

ABSTRACT

The accuracy of numerical results using standard finite element method (FEM) in acoustic problems will deteriorate with increasing frequency due to the "dispersion error". Such dispersion error depends on the balance between the "stiffness" and "mass" of discretization equation systems. This paper reports an improved finite element method (FEM) for solving acoustic problems by re-distributing the mass in the mass matrix to "tune" the balance, aiming to minimize the dispersion errors. This is done by shifting the integration point locations when computing the entries of the mass matrix, while ensuring the mass conservation. The new method is verified through the detailed numerical error analysis, and a strategy is also proposed for the best mass redistribution in terms of minimizing dispersion error. The relative dispersion error of present mass-redistributed finite element method (MR-FEM) is found to be much smaller than the FEM solution, in both theoretical prediction and numerical examination. The present MR-FEM works well by using the linear triangular elements that can be generated automatically, which enables automation in computation and saving computational cost in mesh generation. Numerical examples demonstrate the advantages of MR-FEM, in comparison with the standard FEM using the same triangular meshes and quadrilateral meshes.

1. Introduction

In recent years, with the more and more stringent regulations on noise levels, the need for the design of acoustic systems, such as vehicle and airplane, has attracted more and more attention. In the process of acoustic systems design, the virtual design and prototyping are also becoming more and more important, with the aim to reduce the development time and costs. In the Noise and Vibration (NV) simulations of vehicle, an ideal numerical method should be applicable to all the frequency range, or at least in the audio-frequency range (20 Hz∼20000 Hz). However, most of the numerical prediction techniques for NV analysis are element-based techniques, such as finite element method (FEM) [1] and boundary element method (BEM) [2], which are only confined to low frequency range due to the enhanced dispersion error at high

* Corresponding authors at: State Key Laboratory of Advanced Design and Manufacturing for Vehicle Body, Hunan University, Changsha, 410082, PR China. Fax: +86 73188822051.
E-mail addresses: ericsg2012@gmail.com (E. Li), gyli@hnu.cn (G.Y. Li).
[1] Z.C. He & Eric Li contributed equally to this work.

http://dx.doi.org/10.1016/j.jcp.2016.07.025
0021-9991/

frequency value. There is a so-called "the rule of thumb" which prescribes the "necessary" number of linear finite elements per a wavelength to obtain a reliable solution [3]. However, the number of elements per a wavelength needed for adequately accurate solutions is usually far beyond the value needed by the rule of thumb at high frequency values due to the propagation errors of the waves, which will lead to a big consumption of the computational time.

Actually, the propagation error is closely related to the dispersion errors, which is typically caused by the different wavelength of propagating wave solutions between the discrete and continuous equations. The dispersion reducing techniques for the discretized systems have been studied extensively in the past. In the finite difference schemes, there are several ways to improve the prediction of acoustic problems. The first approach is referred to the dispersion–relation-preserving (DRP) schemes [4]. In the DRP schemes, the finite difference approximations of the space and time derivatives in the wave number and frequency space, are optimized in order to minimize the dispersion error. Such discretizations about the optimization of the scheme coefficients as a function of *wave number* and the grid spacing have were been studied by many other researchers [5–8]. However, the quantity of artificial dissipation required depends on the problem considered. Another approach is to construct higher order schemes [9–11], and the sixth order schemes in [10,11] give very accurate prediction of acoustic wave.

Alternative methods for reducing dispersion error in high frequency range in the finite element frame, a vast amount of research has also been proposed. A survey of finite element methods for time-harmonic acoustics had been provided by Harari [12] and Thompson [13]. In these methods for accurate mid-frequency acoustic analysis, one approach is the use of improved FEMs, such as the Galerkin/least-squares finite element method (GLS-FEM) [14] by using of quadrilateral mesh [15] and linear triangular mesh [16], the quasi-stabilized finite element method (QSFEM) [17], the residual-free finite element method (RFFEM) [18] and discrete Galerkin method [19]. Thompson and Kunthong also proposed a generalized Galerkin least-squares (GGLS) method [20] by adding the residuals, which is the linear combination of Helmholtz residual and gradient residual in least-squares, to the Galerkin variational Helmholtz equation. Another approach is the use of high order approximations, or the so-called p-version FEM. Numerical studies have showed that p-FEM is particularly suitable for accurate solution of acoustic problems [21] and highly nonlinear acoustic fluid [22]. Although the p-FEM can achieve high efficiency in acoustic problems, it also comes with large increase in computational cost, which will make the large-scale simulations prohibitively expensive. Recently, the wave-based method [23], was proposed for acoustic problems with high computational efficiency, while this numerical method is only applicable for the problems with moderate geometrical complexity. That holds back the application in the problems with the complex geometry [24]. Other type of methods, such as the element free Galerkin method (EFGM) [25], the partition of unity method (PUM) [26], the radial point interpolation method (RPIM) [27], the ultra weak variational method (UWVF) [28], the discontinuous enrichment method (DEM) [29] and hybridizable discontinuous Galerkin method (HDG) [30], were also proposed to solve acoustic problems. Compared with the standard FEM, these methods showed a significant improvement of accuracy, while the problem of computational cost has not been solved [31]. It is clear that measures dealing with the root of the dispersion error are required in order to obtain more effective solutions in the acoustic field.

It is well-known that weak form methods such as the FEM and some of the meshfree methods suffer from the "overly-stiff" problem due to the use of standard weak formulations, which generally leads to a significant loss of accuracy in the numerical simulations [32]. This phenomenon is especially true for acoustic (wave propagation) problems, in which the overly-stiff stiffness causes the computed waves propagate with an artificially higher velocity than the real ones in the medium, resulting in the dispersion error in the acoustic simulation [33]. Our previous work has also revealed that the accuracy of the numerical methods in acoustic problems depends on the matching state of the discretized system, such as the "stiffness system" and "mass system" in the undamped dynamic problems. Therefore, one way to tune the balance is to modify (soften) the stiffness of the discretized model.

Liu's group has discovered that the generalized gradient smoothing techniques [34] can effectively soften the overly-stiff of a numerical model, known as the softening effects. The typical softened models include the smoothed finite element methods (S-FEM) [34], and the smoothed point interpolation methods (S-PIM) [35]. The models of S-FEM and S-PIM have been formulated to acoustic problems [36–38]. Innovative means of creating different types of smoothing domains have led to different types of S-FEM and S-PIM models with different levels of softening effects and attractive properties. The study in [39] proved that the numerical wavenumber obtained using node-based smoothed finite element method (NS-FEM) is greater than the actual one, which is in the opposite side of the standard FEM. This phenomenon is mainly caused by the overly-soft stiffness of the node-based smoothed models discovered in [39]. The alpha finite element method (α-FEM) is proposed for acoustic problems [36] by making best use of the "overly-stiff" FEM model and "overly-soft" NS-FEM. By applying the gradient smoothing operation on the constructed edge-based domain, the edge-based smoothed finite element method (ES-FEM) is proposed [37] and formulated for acoustic problems, the mathematical [37] and numerical investigations [38] on the dispersion error of ES-FEM solutions validate that the ES-FEM can give very accurate results especially for acoustic analysis at high frequency values and much better natural eigenfrequencies solutions and frequency response prediction than the FEM does. When it comes to the 3D acoustic problems, the edge-based tetrahedral smoothed finite element method can also provide much more accurate and stable results than the standard FEM using the same tetrahedron mesh and even give more accurate results than the MIR method [38] using hexahedral mesh. All these works showed that by softening the overly-stiff stiffness, which changes the balance between stiffness and mass to enhance the numerical methods' performance on acoustic analysis.

Alternatively, the balance between the stiffness and mass of a discrete model can be tuned by altering the mass matrix. One simple and efficient technique for acoustic and elastic wave propagation problems is based on the calculation of the mass matrix with a weighted average of the most extensively used consistent and lumped mass matrices [41,42]. The bilinear rectangular elements is studied by Guddati and Yue [43] by shifting of the integration points to locations away from traditional Gauss or Gauss–Lobatto integration points for acoustic problems, which results in second-order higher accuracy with respect to dispersion error compared with the conventional integration. Idesman and Pham [44] also developed two finite element techniques based on the modified integration rule for the discretized system matrices and on the averaged mass matrix approaches, and numerical study showed the efficiency of these techniques. All these methods were performed on quadrilateral elements or regular nodes, and the tuning is done for both stiffness and mass matrices. Thompson and Kunthong [12] found that the optimized integration points by making the special quadrature rules for numerical integration equals to the mass matrix obtained from GGLS for equilateral triangles. However, the applicability of this technique to the acoustic problems using a general triangular mesh, and the generally analytic formulae for expressing the locations of integration points in the mass matrix evaluation and its influence on dispersion error in acoustic problems have not been studied.

Motivated by the modified integration rule, in this paper, an alternative approach is proposed to re-distribute the entries in the mass matrix while maintaining the conservation of the total mass for a general linear triangular elements that can be generated automatically. This novel method of mass-redistribution FEM (MR-FEM) is expected to achieve the objective of a perfect balance between the stiffness and mass of the discretization system, which minimizes the dispersion error in the acoustic field. In the present MR-FEM, the stiffness matrix is left alone, but the mass matrix of the discretization system will be modified by shifting the integration points away from the usual Gaussian locations. Our study shows that the present MR-FEM method works ideally for acoustic problems: it can provide much more accurate numerical results compared with the standard FEM and GLS using the same triangular mesh and even the FEM model with quadrilateral mesh.

The paper is organized as follows: Section 2 briefly describes the mathematical model of the acoustic problems. The idea of balancing the generalized mass matrix to the overly-stiff stiffness matrix and the approach to find the locations of the integration points that reduce the dispersion error are discussed in Section 3. The validation of dispersion error for the present MR-FEM method is studied in Section 4. A number of examples are studied in detail to evaluate the performance of the proposed method in Section 5 and finally the conclusions from the numerical results are made in Section 6.

2. Helmholtz equation in acoustic problems

Supposing that the acoustic fluid is inviscid, homogeneous, compressible, and only undergoes small translational movement, the acoustic pressure p' is governed by the wave equation in a bounded domain Ω given as follows:

$$\Delta p' - \frac{1}{c^2}\frac{\partial^2 p'}{\partial t^2} = 0 \quad \text{in } \Omega \tag{1}$$

where Δ is the Laplace operator, c and t are the velocity of sound propagating in the medium and time, respectively. Here the acoustic pressure p' is a small harmonic perturbation around the steady state with the form given as follows:

$$p' = pe^{j\omega t} \tag{2}$$

where ω is the angular frequency, and p is the spatial distribution of complex acoustic pressure and satisfies the following Helmholtz Equation:

$$\Delta p + k^2 p = 0 \tag{3}$$

where k is the wavenumber defined by

$$k = \frac{\omega}{c} \tag{4}$$

For interior acoustic problems, the boundary of the acoustic domain Γ contains three typical kinds Γ_D, Γ_N and Γ_A, where $\Gamma = \Gamma_D \cup \Gamma_N \cup \Gamma_A$. The governing equations for three kinds of boundary conditions are described as follows:

$$p = p_D \qquad \text{on } \Gamma_D \quad \text{Dirichlet condition} \tag{5}$$

$$v = v_n \text{ or } \nabla p \cdot n = -j\rho\omega v_n \qquad \text{on } \Gamma_N \quad \text{Neumann condition} \tag{6}$$

$$v = A_n p \text{ or } \nabla p \cdot n = -j\rho\omega A_n p \qquad \text{on } \Gamma_A \quad \text{Robin condition} \tag{7}$$

where ρ is the density of medium, v_n and A_n represent the normal velocity on the boundary Γ_N and the admittance coefficient on boundary Γ_A, respectively.

3. Modified FEM for acoustic analysis

3.1. A brief on the finite element method (FEM)

In the standard FEM, the acoustic field variable is pressure p, which can be given in the following approximate form:

$$p = \sum_{i=1}^{m} N_i p_i = \mathbf{N}\mathbf{p} \tag{8}$$

where N_i is the shape function of node i obtained using the standard finite element methods and p_i is the unknown nodal pressure. In the standard Galerkin weak form, the weight function w and the shape function $\mathbf{N}$ are the same, and hence the weak form of acoustic problems can be formulated as:

$$-\int_{\Omega} \nabla\mathbf{N}\cdot\nabla\mathbf{N}\mathbf{P}\mathrm{d}\Omega + k^2\int_{\Omega}\mathbf{N}\cdot\mathbf{N}\mathbf{P}\mathrm{d}\Omega - j\rho\omega\int_{\Gamma_N}\mathbf{N}\cdot v_n\mathrm{d}\Gamma - j\rho\omega A_n\int_{\Gamma_A}\mathbf{N}\cdot\mathbf{N}\mathbf{P}\mathrm{d}\Gamma = 0 \tag{9}$$

The discretization system equations can be finally obtained and expressed in matrix form given as follows:

$$\left[\mathbf{K}^{\mathrm{FEM}} - k^2\mathbf{M} + j\rho\omega\mathbf{C}\right]\{\mathbf{P}\} = -j\rho\omega\{\mathbf{F}\} \tag{10}$$

where

$$\mathbf{K}^{\mathrm{FEM}} = \int_{\Omega}(\nabla\mathbf{N})^{\mathrm{T}}(\nabla\mathbf{N})\mathrm{d}\Omega \tag{11}$$

$$\mathbf{M}^{\mathrm{FEM}} = \int_{\Omega}\mathbf{N}^{\mathrm{T}}\mathbf{N}\mathrm{d}\Omega \tag{12}$$

$$\mathbf{C} = \int_{\Gamma_A}\mathbf{N}^{\mathrm{T}}\mathbf{N}A_n\mathrm{d}\Gamma \tag{13}$$

$$\mathbf{F} = \int_{\Gamma_N}\mathbf{N}^{\mathrm{T}}v_n\mathrm{d}\Gamma \tag{14}$$

$$\{\mathbf{P}\}^{\mathrm{T}} = \{p_1, p_2, \cdots, p_n\} \tag{15}$$

where $\mathbf{K}^{\mathrm{FEM}}$ is the acoustical stiffness matrix, $\mathbf{M}^{\mathrm{FEM}}$ is the acoustical mass matrix, $\mathbf{C}$ is the acoustical damping matrix, $\mathbf{F}$ is the acoustical force vector, and $\mathbf{P}$ is the nodal pressure yet to be determined. In the numerical solution of acoustic problems, the stiffness and mass matrices will not change by the boundary conditions. These system matrices can be obtained by assembling the element matrices in the FEM models, which are given by:

$$\mathbf{K}^{\mathrm{e}} = \int_{\Omega^e}(\nabla\mathbf{N})^{\mathrm{T}}(\nabla\mathbf{N})\mathrm{d}\Omega, \tag{16}$$

$$\mathbf{M}^{\mathrm{e}} = \int_{\Omega^e}\mathbf{N}^{\mathrm{T}}\mathbf{N}\mathrm{d}\Omega \tag{17}$$

where Ω^e is the local domain which involves with the element. Note that the only triangular element will be adopted here as it is the best adaptive mesh for any complicated domain discretization.

3.2. Generalized integration rules for evaluation of stiffness and mass matrices

In order to compute the element stiffness and mass matrices shown in Eqs. (16)–(17), the shape functions and the derivation of the shape function should be calculated firstly. For an arbitrary linear triangular element, as shown in Fig. 1, the shape function $\mathbf{N} = [\,N_1 \quad N_2 \quad N_3\,]$ for any arbitrary interior point P with coordinates x and y can be given as follows using the standard approach in FEM [45].

$$\begin{aligned} N_1 &= \frac{1}{2A}\left[(x_2y_3 - x_3y_2) + (y_2 - y_3)x + (x_3 - x_2)y\right] \\ N_2 &= \frac{1}{2A}\left[(x_3y_1 - x_1y_3) + (y_3 - y_1)x + (x_1 - x_3)y\right] \\ N_3 &= \frac{1}{2A}\left[(x_1y_2 - x_2y_1) + (y_1 - y_2)x + (x_2 - x_1)y\right] \end{aligned} \tag{18}$$

where x_i and y_i are the coordinate values at the ith ($i = 1 \sim 3$) node of triangular element, A is the area of the element. The shape function can also be expressed in the form of area coordinates, as shown in Fig. 1. By connecting an arbitrary point P in the interior of the triangle to the three vertices 1, 2, 3, three sub-areas of A_1, A_2, and A_3 corresponding to the triangles P23, P13 and P12 can be determined. The shape functions for the three nodes can then be constructed as:

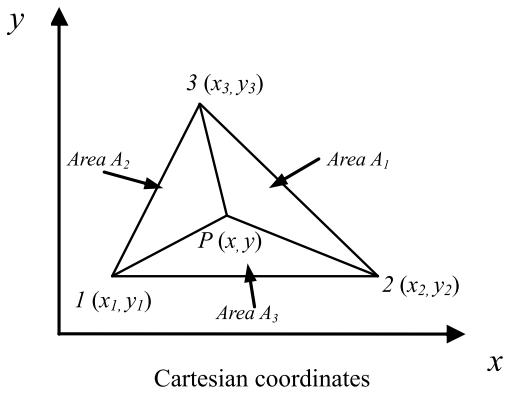

Fig. 1. The illustration of linear triangular coordinates.

$$N_1 = \frac{A_1}{A^e}; \qquad N_2 = \frac{A_2}{A^e}; \qquad N_3 = \frac{A_3}{A^e} \tag{19}$$

where A^e is the area of the triangular.

The derivative of the shape function $\nabla\mathbf{N}$ for linear triangular elements can then be obtained as follows:

$$\nabla\mathbf{N} = \begin{bmatrix} \frac{\partial N_1}{\partial x} & \frac{\partial N_2}{\partial x} & \frac{\partial N_3}{\partial x} \\ \frac{\partial N_1}{\partial y} & \frac{\partial N_2}{\partial y} & \frac{\partial N_3}{\partial y} \end{bmatrix} = \frac{1}{2A}\begin{bmatrix} y_2 - y_3 & y_3 - y_1 & y_1 - y_2 \\ x_3 - x_2 & x_1 - x_3 & x_2 - x_1 \end{bmatrix} \tag{20}$$

Because the derivative of the shape function $\nabla\mathbf{N}$ in Eq. (20) for linear triangular elements is constant, the integration of Eq. (16) becomes the integrand multiplied by the area of the element domain, which is trivial and no numerical integration is needed.

In the calculation of the mass matrix in Eq. (17), the integral function is not constant over the integral domain, and the integration should be calculated analytically (using area coordinate properties [34]), or resolved numerically by using the conventional Gauss integral method:

$$\int_{\Omega^e} \rho\mathbf{N}^{\mathrm{T}}\mathbf{N}\mathrm{d}\Omega = \rho A^e \sum_{i=1}^{ng}\left[w_i\left(\mathbf{N}^{\mathrm{T}}\mathbf{N}\right)_{\text{evaluated at point } i}\right] \tag{21}$$

where ng is the number of Gauss points used to integration, w_i are the weights. For linear triangular element, three Gauss points are adopted to evaluate the mass matrix with the area coordinates of

Point A: $(2/3, \quad 1/6, \quad 1/6)$,

Point B: $(1/6, \quad 2/3, \quad 1/6)$,

Point C: $(1/6, \quad 1/6, \quad 2/3)$

and the weights $w_i = 1/3$ are used for all the three sampling Gauss points. This computational scheme leads to the consistent mass matrix, which is the same as the analytic integration. When the three vertices of triangle are chosen for the integral points with area coordinates of

Point A: $(1 \quad 0 \quad 0)$,

Point B: $(0 \quad 1 \quad 0)$,

Point C: $(0 \quad 0 \quad 1)$.

This method of calculation will lead to the well-known lumped mass matrix. The lumped mass matrix is a diagonal matrix, and thus it is preferred for computations in time-domain, making the system equation solution become efficient at each iteration. It is also noted that in the dynamic problems, both consistent and lumped mass matrix are used extensively, while the "balance" of the mass matrix to the stiffness matrix in the discretized system and its influence on the accuracy of the numerical results have been rarely studied by people.

In this paper, a tunable parameter expressing the integration points locations is used to evaluate the general analytic formula of mass matrix, which also ensures the mass conservation. With such formulation, the objective function of dispersion error is then derived. By minimizing the objective function, the precise locations of the integral points in the triangular element are then determined, which gives a perfect balance between the system mass and stiffness. Therefore, the accuracy of the numerical results is improved significantly in the acoustic discretized system. The general formula of three integration points locations for the mass matrix evaluation is expressed in the following area coordinates:

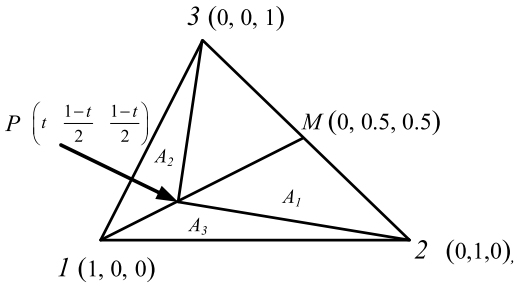

Fig. 2. The illustration of modified integral location in linear triangular element.

$$\begin{aligned}
&\text{Point A:} \quad \left(t \quad \frac{1-t}{2} \quad \frac{1-t}{2}\right)\\
&\text{Point B:} \quad \left(\frac{1-t}{2} \quad t \quad \frac{1-t}{2}\right)\\
&\text{Point C:} \quad \left(\frac{1-t}{2} \quad \frac{1-t}{2} \quad t\right)
\end{aligned} \tag{22}$$

where $t \in [0,1]$, and weight $w_i = 1/3$ making $\sum_{i=1}^{3} w_i = 1$. Note that when t changes from 0 to 1, as shown in Fig. 2, the location of integral point will transfer from a triangle vertex to the midpoint of opposite edge to the vertex. By using the three integral points, the element mass matrix of triangle can be obtained and given in parameter t as:

$$\mathbf{M}^{\mathrm{e}} = \frac{1}{3}A^{e}\begin{bmatrix} t^2+\frac{(1-t)^2}{2} & t(1-t)+\frac{(1-t)^2}{4} & t(1-t)+\frac{(1-t)^2}{4} \\ t(1-t)+\frac{(1-t)^2}{4} & t^2+\frac{(1-t)^2}{2} & t(1-t)+\frac{(1-t)^2}{4} \\ t(1-t)+\frac{(1-t)^2}{4} & t(1-t)+\frac{(1-t)^2}{4} & t^2+\frac{(1-t)^2}{2} \end{bmatrix} \tag{23}$$

It is quite clear that the value obtained by adding together of all elements in matrix of $\mathbf{M}^{\mathrm{e}}$ equals to the triangle area, which is irrelevant to the value of t:

$$\begin{aligned}
\sum \mathbf{M}^{\mathrm{e}} &= \sum_{i=1}^{3}\frac{1}{3}A^{e}\left[\left(t^2+\frac{(1-t)^2}{2}\right)+2\left(t(1-t)+\frac{(1-t)^2}{4}\right)\right]\\
&= A^{e}\left[t^2+(1-t)^2+2t(1-t)\right] = A^{e}\left[t^2+1-2t+t^2+2t-2t^2\right]\\
&= \underbrace{A^{e}}_{\text{total area of the element}}
\end{aligned} \tag{24}$$

It has also been proved in [46] that the overall mass is always conserved, as long as these two requirements are satisfied: 1) the shape functions meet the partitions of unity property; 2) the summation of the weights used for all the integral points is equal to 1. Under these conditions, although the value of mass matrix is affected by the integral points locations, the mass conservation will always be ensured. This rule gives a great freedom to modify the integral points location. It is also easy to find from Eq. (19) that the condition of partitions of unity property is also satisfied for the shape functions.

Up to this point, a general expression to evaluate the mass matrix is successfully obtained, which always guarantees the mass conservation at the element level. Since the individual entries of mass matrix can be "tuned" by the "knob" t, the masses distribution in mass matrix $\mathbf{M}^{\mathrm{e}}$ is greatly influenced by the parameter of t. For this reason, this method is called the "mass-redistributed FEM" or "MR-FEM".

3.3. Dispersion reducing integration for the MR-FEM

It is now ready to tune the knob t, so as to minimize the objective of the dispersion error in our MR-FEM solution. In the discretization of 2D problems using triangular mesh, it is very general and customary to map the finite elements from a parent triangular mesh to the regular triangular mesh by area coordinates form. Here a two dimensional problem is considered, whose domain is discretized with a regular triangular mesh with a constant node spacing h (or the shortest edge in the mesh), as shown in Fig. 3. Then a discretized system in the form of Eq. (10) can be obtained by using MR-FEM with this set of mesh in the analysis of the acoustic problem. In Fig. 3, the nodes which contribute to the MR-FEM system equation involved with interior node (i, j) are also labeled.

The row of equation in the MR-FEM discretization system involves with the node (i, j) which can be written as follows (for free of excitation):

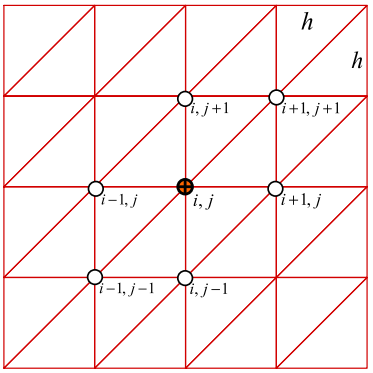

Fig. 3. The Illustration of nodes in constructing system equations involves with node (i, j) in a MR-FEM setting.

$$L_s^{\text{MR-FEM}} = A_1 p_{i,j+1} + A_2 p_{i+1,j+1} + A_1 p_{i-1,j} + A_0 p_{i,j} + A_1 p_{i+1,j} + A_2 p_{i-1,j-1} + A_1 p_{i,j-1} = 0 \tag{25}$$

Here $L_s^{\text{MR-FEM}}$ represents the row of discretized system equation involving with node (i, j) in the MR-FEM. In two-dimensional acoustic problems, the MR-FEM solutions of a plane wave have the following form:

$$p(x) = P_A e^{i(k_1 x + k_2 y)} \quad \text{with } k_1 = k^h \cos\theta,\ k_2 = k^h \sin\theta \tag{26}$$

Substituting Eq. (26) into Eq. (25), leads to

$$\begin{aligned} L_s^{\text{MR-FEM}} &= A_1 e^{i(k_1\cdot 0 + k_2 h)} + A_2 e^{i(k_1 h + k_2 h)} + A_1 e^{i(k_1(-h) + k_2\cdot 0)} + A_0 e^{i(k_1\cdot 0 + k_2\cdot 0)} \\ &\quad + A_1 e^{i(k_1 h + k_2\cdot 0)} + A_2 e^{i(k_1(-h) + k_2(-h))} + A_1 e^{i(k_1\cdot 0 + k_2(-h))} = 0 \end{aligned} \tag{27}$$

After simplification, the real part of $L_s^{\text{MR-FEM}}$ is given as follows:

$$\text{Re}\left(L_s^{\text{MR-FEM}}\right) = A_0 + 2A_1\left(\cos(k_1 h) + \cos(k_2 h)\right) + 2A_2\cos(k_1 h + k_2 h) = 0 \tag{28}$$

with

$$A_0 = 4 - \left[\frac{1 - (2t - 3t^2)}{2}\right]k^2h^2, \qquad A_1 = -1 - \left[\frac{1 + (2t - 3t^2)}{12}\right]k^2h^2, \qquad A_2 = -\left[\frac{1 + (2t - 3t^2)}{12}\right]k^2h^2 \tag{29}$$

and the relation between the actual wavenumber k and the approximated wavenumber k^h can be obtained as

$$k^2 = \frac{1}{h^2}\frac{24 - 12[\cos(k_1 h) + \cos(k_2 h)]}{3(1 - 2t + 3t^2) + (1 + 2t - 3t^2)[\cos(k_1 h) + \cos(k_2 h) + \cos(k_1 h + k_2 h)]} \tag{30}$$

In order to obtain the relative dispersion error, by taking the Taylor expansion of k in terms of k^h. After some simplifications, the dispersion error can be written as

$$k = k^h - \frac{(k^h)^3 h^2}{24}\left(2\cos^4\theta - 2\cos^2\theta + \left(3t^2 - 2t - 1\right)\sin 2\theta + 6t^2 - 4t - 1\right) + o\left(\left(k^h\right)^5\right) \tag{31}$$

By defining the relative dispersion error $e(\theta, k)$ about the difference between the actual wavenumber and the approximated one as:

$$e(\theta, k) = \left|\frac{k - k^h}{k^h}\right| \tag{32}$$

where k is the actual wavenumber and k^h represents the approximated wavenumber. The dispersion error of MR-FEM can be quantified as the relative error which is described as follows:

$$e(\theta, k) = \left|\frac{(k^h)^2 h^2}{24}\left(2\cos^4\theta - 2\cos^2\theta + \left(3t^2 - 2t - 1\right)\sin 2\theta + 6t^2 - 4t - 1\right) + o\left(\left(k^h\right)^4\right)\right| \tag{33}$$

When the dispersion error is small, $k \approx k^h$, and

$$2\left(\cos^4\theta - \cos^2\theta\right) = 2\cos^2\theta\left(\cos^2\theta - 1\right) = -2\cos^2\theta\sin^2\theta = -\frac{1}{2}\sin^2 2\theta \tag{34}$$

It will have

$$e(\theta, k) = \left|\frac{k^2 h^2}{24}\left(-\frac{1}{2}\sin^2 2\theta + \left(3t^2 - 2t - 1\right)\sin 2\theta + 6t^2 - 4t - 1\right) + o\left(k^4\right)\right| \tag{35}$$

Using the above equation, the estimation of the dispersion errors can be obtained for conventional integration rules. When the consistent mass matrix is used (the location parameter of integration point $t = 2/3$), the dispersion error becomes

$$e(\theta, k) = \left| \frac{k^2 h^2}{24} \left(-\frac{1}{2} \sin^2 2\theta - \sin 2\theta - 1 \right) + o\left(k^4\right) \right| \tag{36}$$

The leading error (the quadratic term) is bounded by $|-\frac{1}{2}\sin^2 2\theta - \sin 2\theta - 1| \leq \frac{5}{2}$. When the lumped mass matrix is used (the location parameter of integration point $t = 1$), an analogous result is obtained

$$e(\theta, k) = \left| \frac{k^2 h^2}{24} \left(-\frac{1}{2} \sin^2 2\theta + 1 \right) + o\left(k^4\right) \right| \tag{37}$$

In this case, the leading error (the quadratic term) is bounded by $|-\frac{1}{2}\sin^2 2\theta + 1| \leq 1$.

It can be found in Eqs. (36)–(37) that the magnitude of leading error for the consistent mass matrix formulation is larger than that of the lumped mass formulation. If the term of $6t^2 - 4t - 1$ in Eq. (35) is equal to zero, the dispersion error term will become

$$e(\theta, k) = \left| \frac{k^2 h^2}{24} \left(-\frac{1}{2} \sin^2 2\theta - \frac{1}{2} \sin 2\theta \right) + o\left(k^4\right) \right| \tag{38}$$

In this case, the leading error (the quadratic term) is bounded by $|-\frac{1}{2}\sin^2 2\theta - \frac{1}{2}\sin 2\theta| \leq 1$. The optimal value of t becomes: $t = \frac{4 \pm \sqrt{16+4\times 6}}{12} = \frac{2 \pm \sqrt{10}}{6}$. Because $t \in [0, 1]$, it will finally get

$$t = \frac{2 + \sqrt{10}}{6} \tag{39}$$

It can be seen from the derivation that the leading error (the quadratic term) of MR-FEM is identical to the FEM using lumped mass matrix, and smaller than the FEM using consistent mass matrix, while due to wavenumber assumption, i.e. $k \approx k^h$ in Eq. (35), the leading error of the MR-FEM and FEM using consistent mass matrix is larger than the actual error, while the leading error of the FEM using lumped mass matrix is smaller than the actual error, and thus the MR-FEM provides the best results. The validation of this conclusion is given in the next section.

It is found that the three Gauss points locations for this type mesh are identical to the special quadrature rules proposed by Thompson and Kunthong [12], who found this conclusion by making the numerical integration of mass matrix equal to the mass matrix obtained from GGLS using a canonical periodic mesh with a patch of six equilateral triangular. This also can verify that the MR-FEM is suitable to other types of mesh topology. By substituting the optimized Gauss point location Eq. (39) into Eq. (23), it can also be found that the optimized Gauss point location for triangular mesh will lead to the mass matrix that is identical to the averaging of consistent and lumped mass matrix. The conclusion is similar to the work of Marfurt [40] in 1D and 2D quadrilateral mesh in frequency domain problems.

4. Dispersion error spectrum analysis for MR-FEM

4.1. Dispersion spectrum validation of FEM and MR-FEM

Noted that the relative dispersion error $e(\theta, k)$ in Eq. (35) has been derived under the assumption of $k \approx k^h$, when it comes to large wavenumber, i.e. $k > 1$, the dispersion error will increase dramatically, and thus the assumption is no longer held. In this section, the validation of theoretical analysis in section 3.3 using the numerical dispersion analysis is also conducted. Since the exact wavenumber in 2D problems satisfies the standard equation of circle, while it can easily be confirmed that Eq. (28) is not an equation of circle, indicating that the solution of numerical wavenumber using MR-FEM always has the dispersion error. It can also be seen that the dispersion error in the MR-FEM model also depends on both direction of wave propagation and wavenumber. In addition, it is observed from Eq. (28) that the numerical wavenumber is about origin symmetric in the (k_1, k_2) plane, so only the wave propagation angles from 0° to 180° are necessary to study. The full spectrum of the dispersion error for MR-FEM with wave propagation angle values of θ from 0° to 180° is examined, in comparison with that of FEM using the consistent and lumped mass matrix.

The relative dispersion error of MR-FEM can be computed by solving Eq. (28) with a specific Gauss point location, or obtained using Eq. (35). Because the numerical wavenumber obtained using Eq. (28) is very close to the actual numerical wavenumber, the "Exact solution" denotes the relative dispersion error obtained by solving Eq. (28) directly, while the "Taylor expansion" represents the relative dispersion error obtained by computing Eq. (35). Fig. 4 plots the relative dispersion errors for both FEM with different mass matrix and the MR-FEM with respect to direction and wavenumber. As shown in the figures, the "Exact solution" and "Taylor expansion" agree well with each other when kh is relatively small. However, with the increase of kh, the deviation between the "Exact solution" and "Taylor expansion" can be observed, i.e. the relative dispersion error of FEM with consistent mass matrix and MR-FEM obtained using Taylor expansion is larger than the exact, while the relative dispersion error of FEM with lumped mass matrix obtained using Taylor expansion is smaller than the exact. It can also be indicated that the FEM using lumped mass matrix gives larger dispersion error compared with FEM

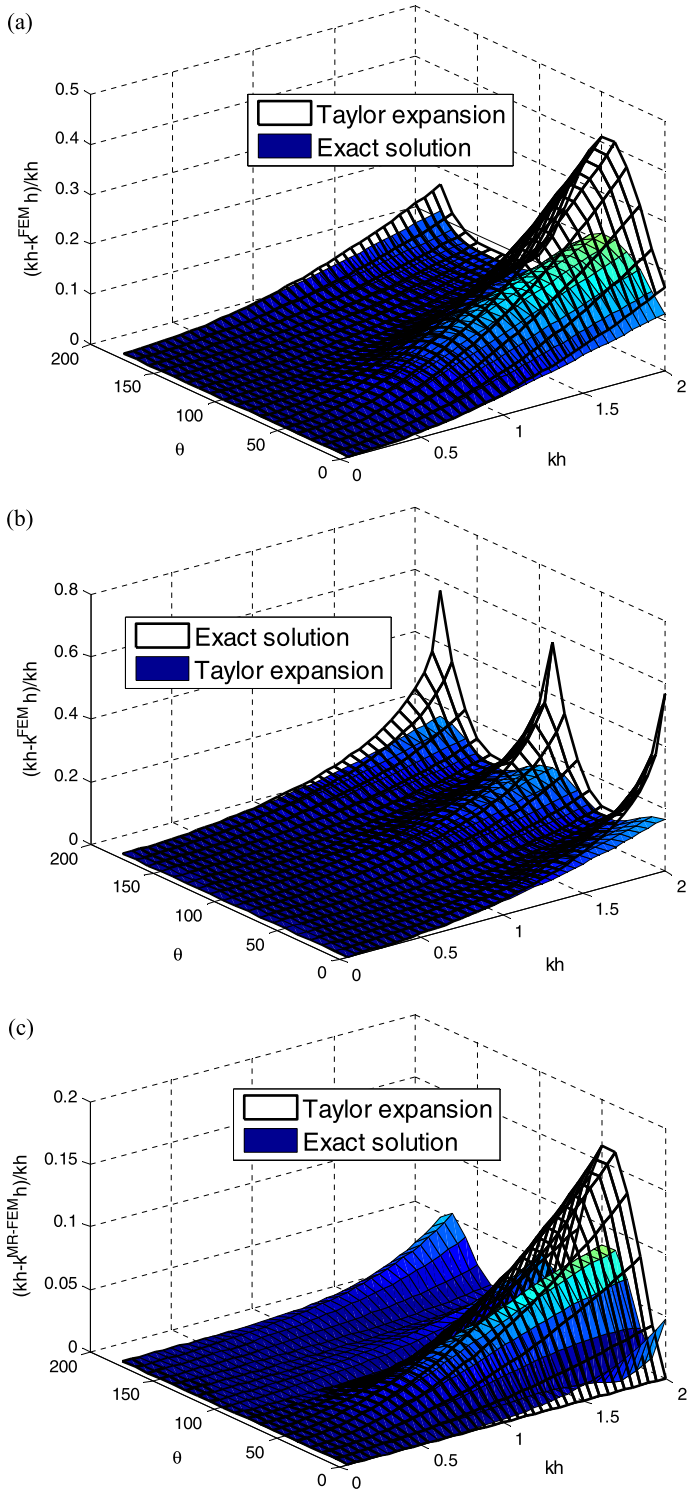

Fig. 4. Validation of dispersion error over θ and kh for FEM and MR-FEM: (a) FEM using consistent mass matrix, (b) FEM using lumped mass matrix, (c) MR-FEM.

using consistent mass matrix at higher wavenumber. It can also be found from the exact solution that: compared with the FEM solution using consistent mass matrix, a significant improvement can be observed for the MR-FEM at higher wavenumber in terms of dispersion error, i.e. $kh = 2$, the dispersion error of MR-FEM solution is one third of the FEM solution using consistent mass matrix.

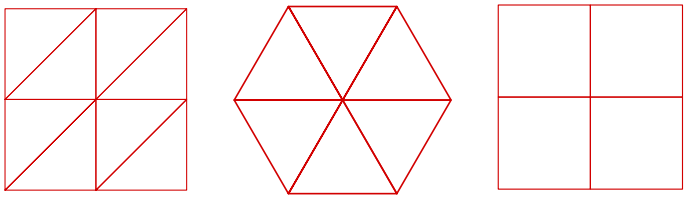

Fig. 5. Different meshes topology with constant node spacing of h.

4.2. Influence of the triangular mesh topology on MR-FEM

In this section, the effect of the mesh topology on the dispersion error of the MR-FEM is also studied. Two kinds of triangular mesh called regular mesh and hexagonal mesh, which are usually used in the mesh generation of commercial software, i.e. Hypermesh for the complex geometry, are adopted to study. In order to make comparisons, the GLS-T3 and FEM with two kinds of mass matrix using the same set of triangular mesh and the FEM using quadrilateral mesh are also used for the comparison. The mesh topologies are all shown in Fig. 5, and all these topologies have a constant mesh size of h.

The dispersion errors of different mesh topologies for these numerical methods are studied at two different wavenumber values of kh ($kh = 0.5, 1.0$), and the computed results are all plotted in Fig. 6. The following points can be observed:

- With the increase of kh, the dispersion error of FEM, GLS-T3 and MR-FEM will increase for all these three types of meshes.
- Among the two kinds of triangular topologies studied, the FEM, GLS-T3 and MR-FEM using hexagonal mesh can obtain much smaller dispersion error than them using regular mesh. It can also be found that the error of FEM (Lump) is smaller than FEM (Cons) by using regular mesh when the wavenumber is relative small, i.e. $kh \leq 1$; For hexagonal mesh, the FEM (Lump) always gives worse results than FEM (Cons).
- With the two values of wavenumber for the two types of triangular meshes, the GLS-T3 can improve the accuracy of FEM, while the MR-FEM provides the best results among GLS-T3, FEM-T3 and FEM with quadrilateral elements in the cases of both low and high wavenumber, indicating that the MR-FEM is very suitable for acoustic analysis.

5. Numerical example

5.1. Numerical error

In this paper, the numerical error indicator for acoustic problems is always estimated in terms of velocity, which has the following form:

$$\left|p^e - p^h\right|_1^2 = \int_{\Omega} \left(\tilde{v}^e - \tilde{v}^h\right)^{\mathrm{T}} \left(v^e - v^h\right) \mathrm{d}\Omega \tag{40}$$

where $\tilde{v}$ denotes complex conjugate of the velocity v, the superscript e is the exact velocity and h is the numerical solutions obtained from numerical methods, including the present MR-FEM, Galerkin/least-squares finite element method (GLS) and FEM using triangular mesh with linear interpolation and FEM using the quadrilateral mesh with bilinear interpolation for the shape function. In this paper, the FEM (Cons) and FEM (Lump) represent the FEM using consistent mass matrix and lumped mass matrix, respectively. It was shown by Ihlenburg in [1] that the numerical relative error of acoustic problems can be estimated using a uniform hp-mesh for FEM model:

$$\eta = \sqrt{\frac{\int_{\Omega} (\tilde{v}^{exact} - \tilde{v}^h)^{\mathrm{T}} (v^{exact} - v^h) \mathrm{d}\Omega}{\int_{\Omega} \tilde{v}^{exact} v^{exact} \mathrm{d}\Omega}} \leq C_1' \left(\frac{kh}{2p}\right)^p + C_2' k \left(\frac{kh}{2p}\right)^{2p} \tag{41}$$

where C_1' and C_2' are constant regardless of the wavenumber k and mesh size h, and p denotes the polynomial approximation degree used in the discretization model. The relative numerical error contains two terms: the first term is *interpolation error* and the second term is *pollution error* which is the most concerned in acoustic simulation problems. The relative error of acoustic problems using FEM is bounded as follows in the case of $kh < 1$ [1]:

$$\eta \leq C_1 kh + C_2 k^3 h^2 \tag{42}$$

In this paper, the non-dimensional treatment is also introduced, and the wave number in the following sections is expressed in a non-dimensional wave number k. The relation of between non-dimensional coordinates and the 2D Cartesian coordinates are defined by the

$$\xi = x/l, \qquad \zeta = y/l \tag{43}$$

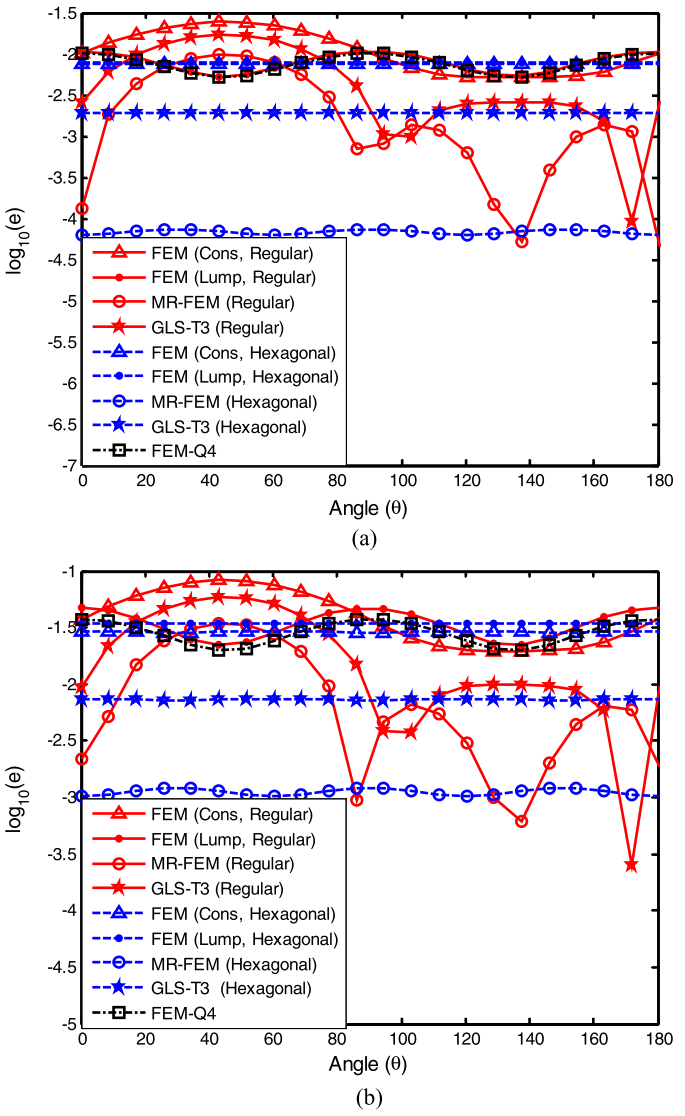

Fig. 6. Comparison the dispersion error for FEM and MR-FEM using different mesh topologies: (a) $kh = 0.5$ (about twelve elements per wavelength), (b) $kh = 1$ (about six elements per wavelength).

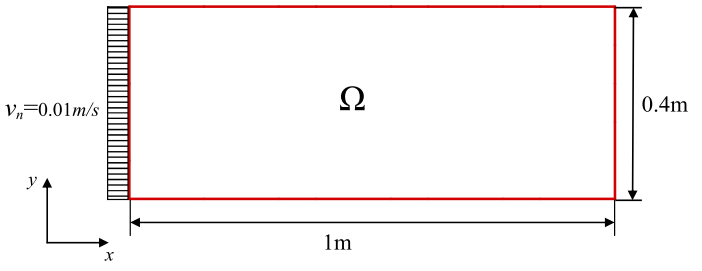

Fig. 7. The illustration of 2D acoustic tube and boundary condition.

5.2. Numerical example 1: 2D problem with Neumann boundary condition

The first numerical example, adopted to verify the present MR-FEM, has an analytical solution. The acoustic domain is a 2D rectangular tube filled with air, as shown in Fig. 7. The tube has the dimensions of length $l = 1$ m and width $b = 0.4$ m. The left of the tube is subjected to normal velocity with $v_n = 0.01$ m/s, and the other boundaries of the tube are rigid wall.

The air density ρ is 1.225 kg/m^3 and the velocity of sound propagating in the air is 340 m/s. The pressure and velocity have analytical solutions for this problem, which are expressed as:

$$p = -j\rho c v_n \frac{\cos(k(1-\xi))}{\sin(k)} \tag{44}$$

$$v = \frac{v_n \sin(k(1-\xi))}{\sin(k)} \tag{45}$$

The 2D tube with rigid walls has following natural eigenfrequencies corresponding to the values:

$$f = \frac{c}{2}\sqrt{\left(\frac{m}{l}\right)^2 + \left(\frac{n}{b}\right)^2} \quad m = 0, 1, 2\cdots,\ n = 0, 1, 2\cdots \tag{46}$$

f here are the exact natural eigenfrequencies for this 2D tube, m and n are the corresponding modal order in the x- and y-axis.

5.2.1. Numerical error and convergence

In this numerical example, the performance of present MR-FEM is investigated compared with FEM and GLS using triangular (T3) elements and FEM using quadrilateral (Q4) elements. The convergence property of present MR-FEM is firstly studied. Four models with 55, 87, 189 and 697 uniformly distributed nodes are adopted, and their mesh size are 0.1 m, 0.08 m, 0.05 m and 0.025 m, respectively. Fig. 8(a) plots the convergence curves of numerical error according to Eq. (40) against the average nodal spacing h at frequency of 600 Hz for different methods. It is shown in the figure that the monotonic convergence can be obtained for FEM-T3 (Cons), FEM-T3 (Lump), GLS-T3, MR-FEM and FEM-Q4. While the result of FEM-Q4 is less accurate than that of FEM-T3 (Cons) for this specific problem, this is because the dispersion error of FEM-T3 (Cons) is smaller than the FEM-Q4 when the wave propagating angle is equal to 0° (or wave propagates along the direction of *x-axis*). It can also be observed in Fig. 8(a) that the FEM-T3 shows a higher convergence rate than the FEM-Q4 at frequency of 600 Hz, this is because the numerical error of FEM-T3 is very large in the case of $kh > 1$, and the solution of convergence rate appears larger than it should be. This does not give the true convergence rate for FEM-T3. To examine the true convergence rate, a smaller wavenumber should be used, so that the error is determined mainly by the size of the element. It is shown in Fig. 8(b), when the frequency of 542 Hz ($kh \leq 1$) is used, it is now clear that the convergence of FEM-T3 (Cons) is similar to those of MR-FEM, GLS-T3 and FEM-Q4. It can also be indicated in the figures that the results of these methods at the frequency of 542 Hz ($kh \leq 1$) are not as accurate as the ones at the frequency of 600 Hz ($kh > 1$), this is because the frequency of 542 Hz is close to the eigenfrequency of 544 Hz, which is indicated in Table 1, making the estimated error become larger for all numerical methods. These studies show that the present MR-FEM can always provide much more accurate gradient results than those of FEM-T3 (Cons), FEM-T3 (Lump), GLS-T3 and FEM-Q4.

5.2.2. Acoustic natural eigenfrequency analysis

In the early development of products, the acoustic modal quantities, i.e., eigenfrequencies, eigenmodes can be predicted by numerical methods. It is known that the stiffness of standard FEM model behaves much stiffer than the exact, leading to large error of eigenfrequencies prediction. In this section, the undamped acoustic natural eigenfrequencies analysis is also conducted. Two types of meshes using triangular and quadrilateral elements with same number of nodes and same average mesh size of 0.1 m are also used, which is shown in Fig. 9. The average mesh size of 0.1 m guarantees a frequency limit of 542 Hz under the "the rule of thumb". Table 1 lists the first fifteen natural eigenfrequencies obtained using MR-FEM, FEM-T3 (Cons), FEM-T3 (Lump) and FEM-Q4. In order to make a comparison, the analytical solutions are also listed in the table. As indicated in Table 1, the FEM using consistent mass matrices (including triangular and quadrilateral mesh) generally provides larger eigenfrequencies prediction compared to the exact, while the FEM using lumped mass matrices provides smaller eigenfrequencies prediction compared to the exact. Due to the perfect balanced system matrix conducted in the MR-FEM, the MR-FEM model can provide much more accurate eigenfrequencies solutions than the FEM using the same set of triangular mesh, and even more accurate than the FEM using quadrilateral mesh. The results are becoming more obviously at higher order infrequencies.

5.2.3. Effects of nodal irregularity

In real engineering problems, it is impossible to discretize the domain into regular nodes for the complex domain. In order to evaluate the effects of the mesh irregularities on the numerical results, the comparisons between the regular and irregular mesh using MR-FEM, GLS and FEM with consistent mass matrix are conducted in this numerical example. Two mesh models with regular and irregular node distribution are presented in Fig. 10, and the frequency value of 500 Hz ($k = 9.24$, $kh = 0.74$) is adopted. The acoustic pressures distributions at the bottom of tube are investigated in detail. Fig. 11 plots the acoustic pressures along the *x-axis* obtained using MR-FEM with these two types of mesh. For the purpose of comparison, the results of GLS and FEM using consistent mass matrix are also presented together with the *exact* solution. Note that this problem has an analytical solution of eigenvalues corresponding to the wavenumber $k = \pi n$, $n \in N$, as shown in Eq. (43). In the vicinity of the eigenvalues, the problem will becomes ill-posed in the numerical simulation, with numerical error increases significantly. The wavenumber of 500 Hz is 9.24, which is near the eigenvalue of 9.42 for this problem. In

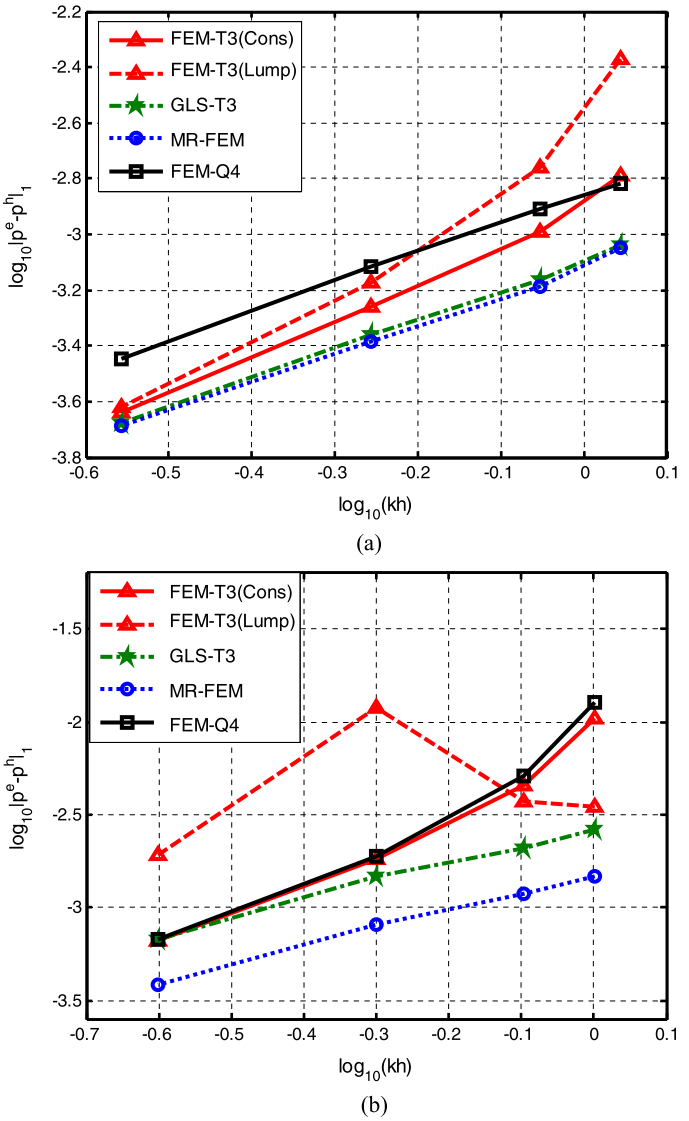

Fig. 8. Comparison of numerical error and convergence: (a) 600 Hz, (b) 542 Hz.

Table 1
2D tube natural eigenfrequencies calculated by FEM and MR-FEM.

Eigenvalue	Exact (Hz)	FEM-T3 (Cons)		FEM-T3 (Lump)		MR-FEM-T3		FEM-Q4	
		Eigenfre	Error (%)	Eigenfre	Error (%)	Eigenfre	Error (%)	Eigenfre	Error (%)
1	170	170.67	0.394	169.270	0.429	169.96	0.024	170.7	0.412
2	340	345.31	1.562	334.140	1.724	339.65	0.103	345.62	1.653
3	425	435.59	2.492	413.750	2.647	424.27	0.172	435.99	2.586
4	457.74	473.54	3.452	446.380	2.482	459.33	0.347	468.22	2.290
5	510	527.41	3.414	490.400	3.843	508.47	0.300	529.02	3.729
6[a]	544.27	576.08	5.845	530.120	2.600	551.3	1.292	556.36	2.221
7[a]	663.87	709.39	6.857	630.740	4.990	673.25	1.413	685.53	3.263
8[a]	680	732.18	7.674	641.270	5.696	676.61	0.499	725.09	6.631
9[a]	801.89	881.81	9.966	747.270	6.811	812.15	1.279	846.08	5.511
10[a]	850	934.48	9.939	760.130	10.573	833.93	1.891	937.26	10.266
11[a]	850	938.18	10.374	762.240	10.325	835.68	1.685	937.26	10.266
12[a]	866.83	961.51	10.923	782.760	9.699	857.11	1.121	952.68	9.904
13[a]	915.48	1034.9	13.045	822.260	10.183	912.85	0.287	998.95	9.118
14[a]	950.33	1077.7	13.403	855.110	10.020	953.43	0.326	1033.7	8.773
15[a]	991.26	1162.6	17.285	875.170	11.711	987.59	0.370	1076.3	8.579

[a] The frequencies do not satisfy the rule of thumb of the relation between the frequency and mesh size.

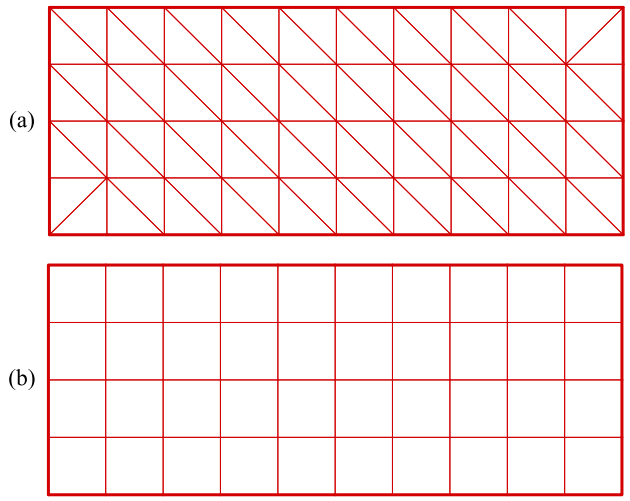

Fig. 9. Domain discretizations of a tube using triangular and 4-node quadrilateral elements.

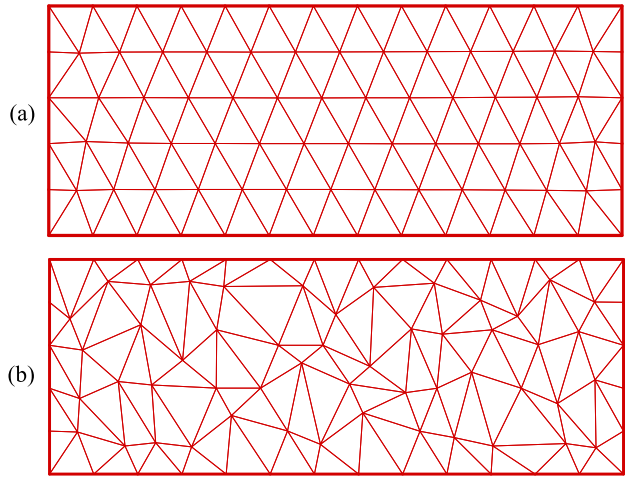

Fig. 10. Two meshes with regular and irregular node distribution: (a) regular mesh, (b) irregular mesh.

addition, the dispersion error is relatively small when the wave propagation angle equals to zero in the case of $kh < 1$. These are the reasons why the numerical error here is mainly the amplitude error. In this numerical example, the picture shows that both MR-FEM and FEM results are influenced by the mesh irregularities, while the result of GLS is more sensitive to the mesh distortion. It is also found that the MR-FEM can always provide much more accurate results than the FEM using both regular and irregular mesh even in the vicinity of the eigenvalues, which implies that the present MR-FEM is more potential to extend in many engineering problems.

5.3. Muffler prediction

The muffler is an acoustic soundproofing device for reducing noise emitted by the exhaust of engine, and has been widely used in the engineering. In this example, a simple expansion chamber is used to verify the present MR-FEM. The dimensions of the muffler are shown in Fig. 12, and the left of muffler is the inlet with a uniform normal velocity $v_n = 1$ m/s, the right end of muffler is outlet with admittance $A_n = 1/\rho c$, the rest boundaries of the muffler are assumed to be rigid. The acoustic fluid is air and the parameters are the same as the previous one. In the performance evaluation of a muffler, one of the most important indicators is transmission loss (TL), which is defined as follows:

$$TL = 10 \lg \frac{W_i}{W_o} \quad \text{with } W = \int_{\partial\Omega} \frac{|p|^2}{2\rho c} dA \tag{47}$$

where W_i and W_o represent the incident and transmitted power, respectively.

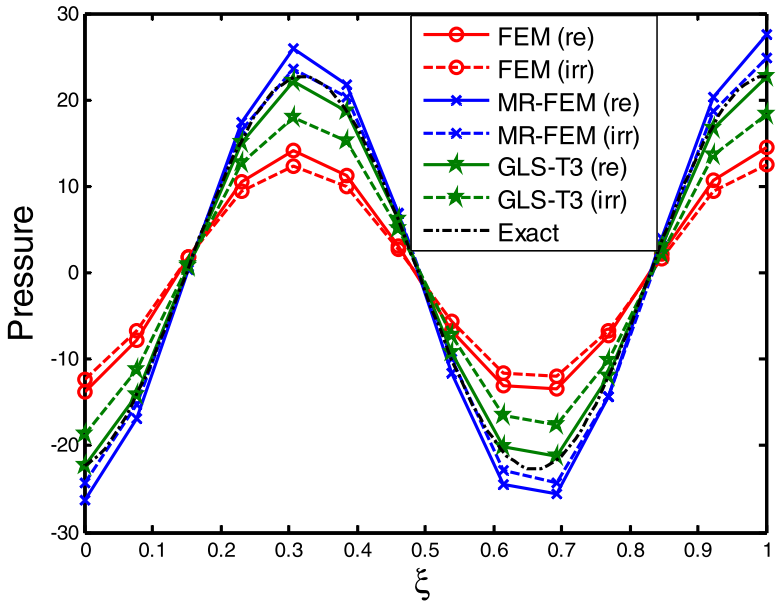

Fig. 11. Acoustic pressure distribution obtained using different methods along the *x-axis* at 500 Hz.

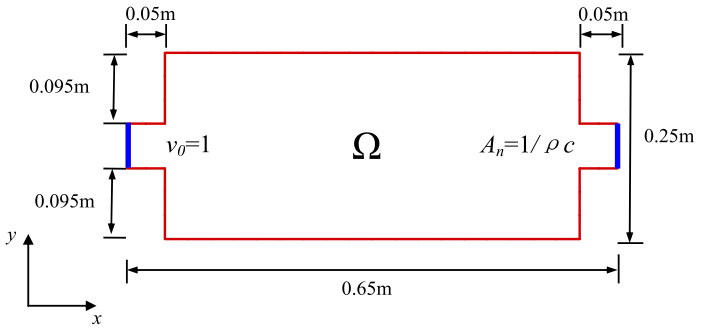

Fig. 12. 2D expansion chamber of muffler with boundary conditions.

5.3.1. Acoustic error and transmission loss

The muffler is discretized into triangular and quadrilateral mesh with an average mesh size of 0.03 m. The acoustic pressure distribution at frequency of 1500 Hz ($kh = 0.83$, about five elements per wavelength) is firstly investigated. Fig. 13 presents the contour of acoustic pressure obtained from MR-FEM, FEM-T3 (Cons), FEM-T3 (Lump), GLS-T3 and FEM-Q4 at the same scale. As the problem does not have analytical solutions, a reference configuration using FEM with a very fine mesh (59435 nodes with 58853 quadrilateral elements) is adopted and the result is also presented in Fig. 13. It can be seen from these contours that the results of FEM using both triangular and quadrilateral meshes show the obvious dispersion, while the contours of GLS and MR-FEM using triangular mesh are very close to the reference result. By making a comparison between GLS-T3 and MR-FEM, the MR-FEM provides more accurate result than the GLS-T3.

Fig. 14 plots the transmission loss obtained using MR-FEM and GLS-T3 using a discretization model of 193 nodes with frequency range from 700 Hz to 1800 Hz. In order to make a comparison, the results of FEM with different mass matrices using a mesh of 193 nodes and 2745 nodes are all plotted in the figure. As shown in the figure, all results are similar in the lower frequency range. However, when it comes to higher frequency range, the results of MR-FEM using 193 nodes are very close to the FEM result using 2745 nodes, while the results of FEM with different mass matrices and GLS-T3 using 193 nodes deviate a lot from that of FEM with finer mesh. This also validates that the MR-FEM can provide much better results than the FEM using the same set of mesh and even close to FEM results using fine mesh.

5.3.2. Convergence and computational efficiency

The convergence property is also investigated in this problem, and three unstructured mesh models are used with an average mesh size of 0.03 m, 0.015 m and 0.0075 m. Fig. 15 plots the numerical error against the average nodal spacing h at frequency of 1500 Hz for FEM-T3 (Cons), FEM-T3 (Lump), GLS-T3, MR-FEM and FEM-Q4. From this figure, it can be observed that the numerical errors converge with the refinement of mesh for all five methods. It can also be seen from this figure

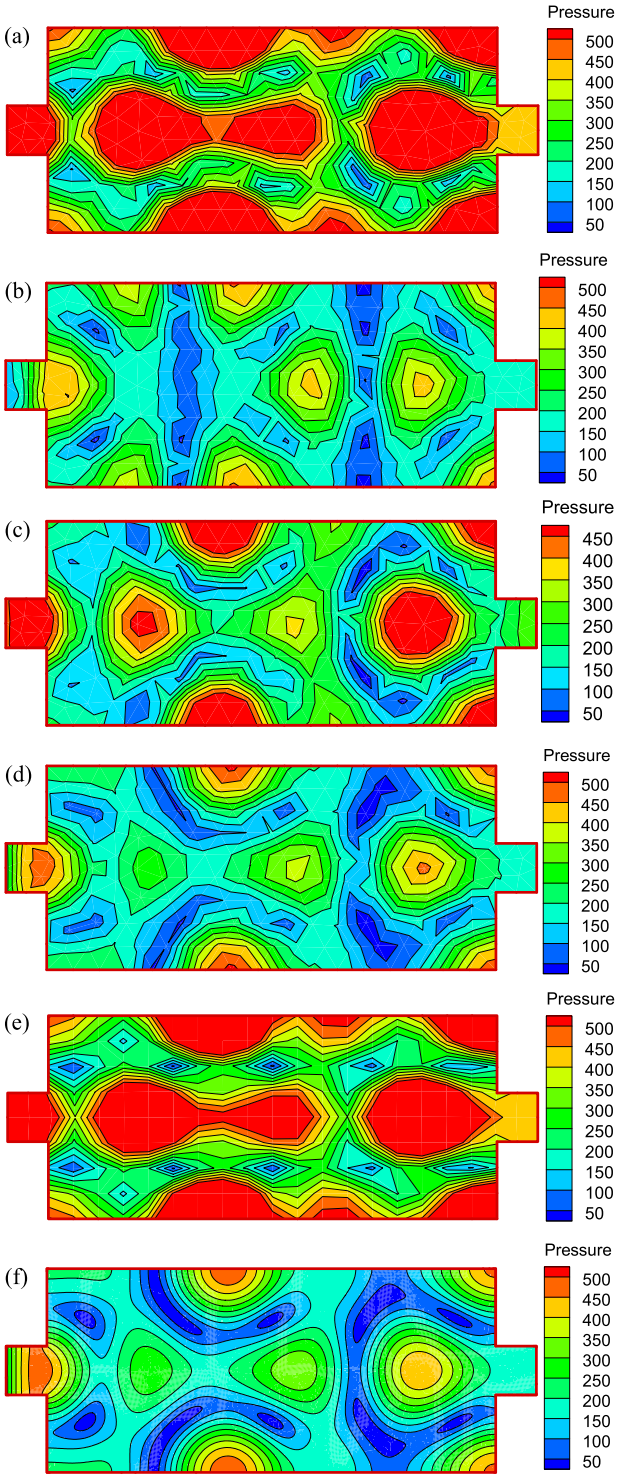

Fig. 13. Distribution of the acoustic pressure with the wavenumber $kh = 0.83$ (about five elements per wavelength): (a) FEM-T3 (Cons), (b) FEM-T3 (Lump), (c) GLS-T3, (d) MR-FEM (e) FEM-Q4, (f) Reference.

that the FEM-Q4 provides smaller numerical error than the FEM-T3 (Cons), and converges faster than the FEM-T3 (Lump), GLS-T3 and MR-FEM, while the MR-FEM can give the best results among these five methods. Note that the discretization models are based on the unstructured mesh with grids not uniform distributed, which leads to poor solution of GLS.

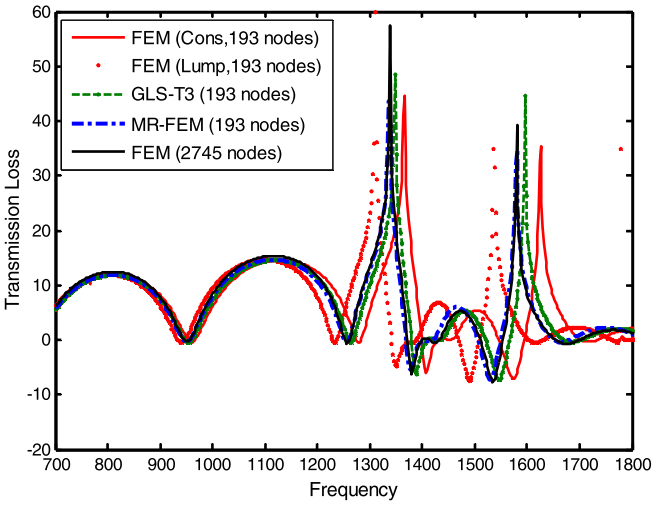

Fig. 14. Transmission loss prediction using different numerical methods.

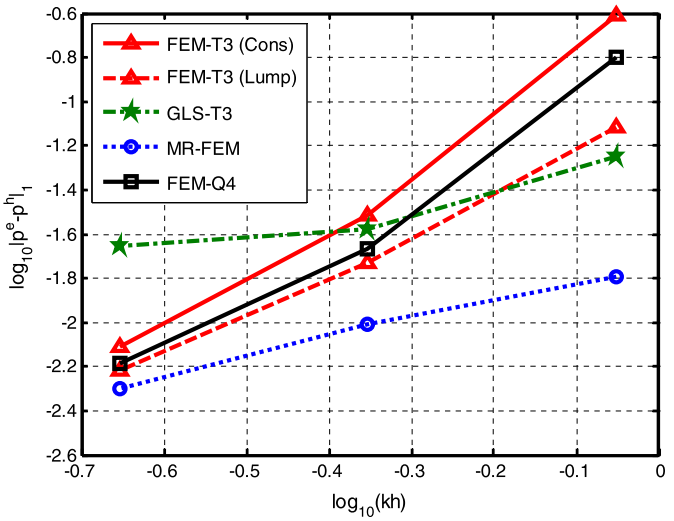

Fig. 15. Comparison of the computational time for the MR-FEM and FEM.

The efficiency of present MR-FEM, FEM-T3 (Cons), FEM-T3 (Lump), GLS-T3 and FEM-Q4 are also investigated in this numerical example. Fig. 16 compares the computational time for FEM-T3, GLS-T3, MR-FEM and FEM-Q4. It is seemed that the MR-FEM takes almost the same amount of time to solve as the FEM using triangular mesh, and a shorter time than GLS-T3 and the FEM-Q4 with the same number of nodes. This is because the bandwidth of MR-FEM is the same as the FEM using triangular mesh and is smaller than the FEM using quadrilateral mesh. The conclusion that the bandwidth of MR-FEM is 7/9 of the bandwidth of the FEM using the quadrilateral mesh can easily be derived in Fig. 3. In addition, the number of sample points required by the Gauss rule for triangular element is less than the number of sample points for the quadrilateral element in the processing the stiffness and the mass matrix integration. These are the reasons why the MR-FEM costs less time than the FEM using quadrilateral mesh. Note that the bandwidth of GLS-T3 is also the same as the FEM using triangular mesh, while the mesh parameter calculation in GLS also increases the computational time, thus the GLS spends a little more time than the FEM using triangular mesh. It is also found that the MR-FEM is more efficient than the FEM-T3, GLS-T3 and FEM-Q4 in terms of CPU time for the same accuracy as shown in Fig. 17.

5.4. 2D multi-fluids acoustic problem

In the practical, an engineer is usually faced with the analysis of a problem where two or more different physical systems, and these different physical systems interact with each other. Often, there is no analytical for the couple systems, and thus numerical methods are usually employed. In this section, the propagation of acoustic waves through a tube with multi-fluids is analyzed. The tube is subjected to essential boundary condition at one side of the tube with $p = 1$, and with

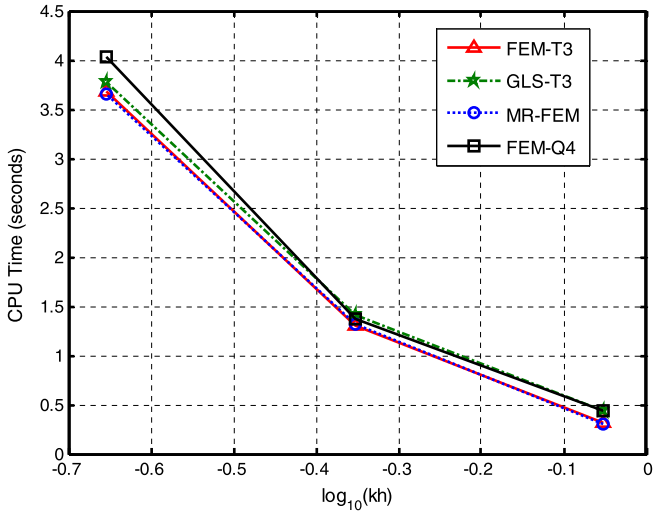

Fig. 16. Comparison of the computational time for different methods.

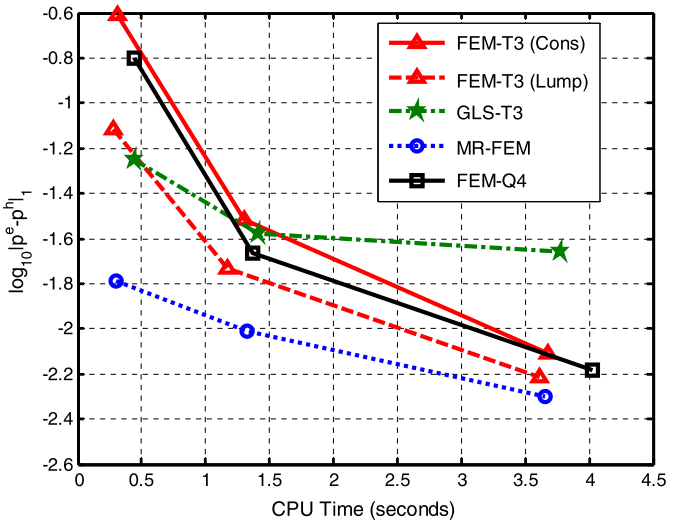

Fig. 17. Comparison of the efficiency for different methods.

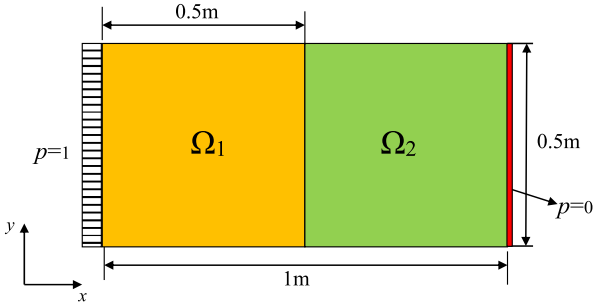

Fig. 18. The illustration of 2D multi-fluid domain and boundary condition.

$p = 0$ at the opposite end, as shown in Fig. 18. The properties of the media are: Medium 1 (Ω_1): density $\rho_1 = 1.225$ kg/m^3 and $c_1 = 200.0$ m/s; Medium 2 (Ω_2) : $\rho_2 = 1.225$ kg/m^3 and $c_2 = 400.0$ m/s.

In order to study the performance of MR-FEM in multi-fluids domain, the comparison between the MR-FEM and FEM using triangular mesh or quadrilateral mesh is studied in this section. The domain is discretized into 231 nodes with node spacing of 0.1 m. The numerical results of FEM (T3), FEM (Q4) and MR-FEM are presented in Fig. 19, with a reference result

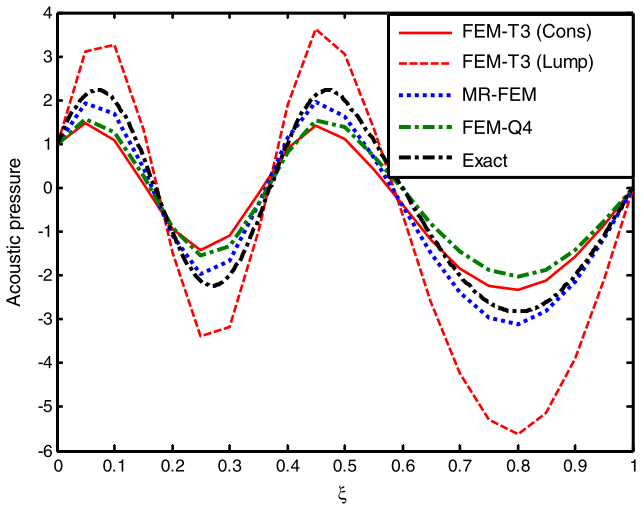

Fig. 19. Comparison of the accuracy of different methods at frequency of 500 Hz.

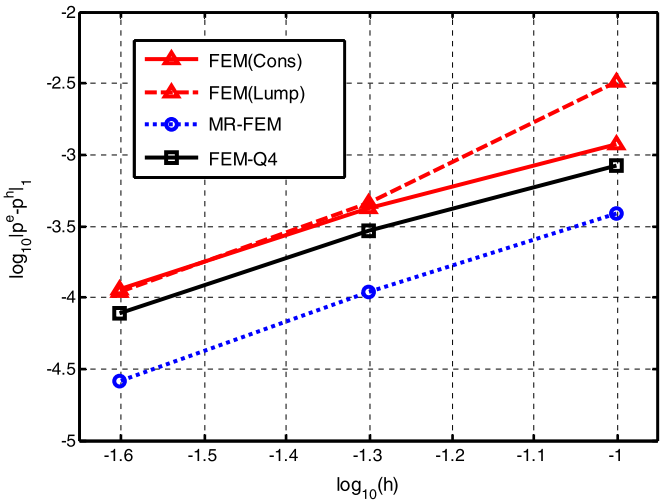

Fig. 20. Comparison of the convergence for the MR-FEM and FEM.

obtained using FEM with a very fine mesh (80601 nodes with node spacing of 0.05 m). It can be easily seen from the figure that the MR-FEM can give much better prediction than the FEM using both triangular and quadrilateral meshes. The convergence property is also studied in this problem, and three unstructured mesh models are used with an average mesh size of 0.1 m, 0.05 m and 0.025 m. Fig. 20 plots the numerical error against the average nodal spacing h at frequency of 500 Hz for FEM-T3 (Cons), FEM-T3 (Lump), MR-FEM and FEM-Q4. From this figure, it can be observed that the numerical solutions from all methods converge with the refinement of mesh, but MR-FEM gives the best results among these methods.

5.5. 2D car acoustic problem

The acoustic characteristics of automobile passenger compartment, which has been frequently used as a benchmark in acoustic simulation, is also adopted to study the accuracy of MR-FEM. Fig. 21 illustrates the 2D geometry of interior cavity for a Multi-Purpose Vehicles (MPV). The acoustical fluid is air and the parameters are identical to the problem in Section 5.3. As the Front-engine and Front-wheel drive layout are adopted in this MPV, the main source of generating noise in the vehicle passenger compartment comes from the engine in the front of firewall. The boundary conditions are then described as: the front firewall is subjected to the vibration with normal velocity of 0.01 m/s, and the passenger compartment roof is fixed with absorbing material with admittance of 0.00144 $m^3/(Pa\,s)$.

The frequency response analysis is used extensively in the NV simulations, and the direct frequency response analysis at the driver's ear point is also conducted using present MR-FEM, FEM and GLS with Neumann and Admittance boundary conditions shown in Fig. 21. The interior cavity of MPV is discretized into 496 nodes with 820 triangular elements and the average mesh size is 0.1 m, giving a frequency limit of 541 Hz based on the "rule of thumb". Fig. 22 plots the responses

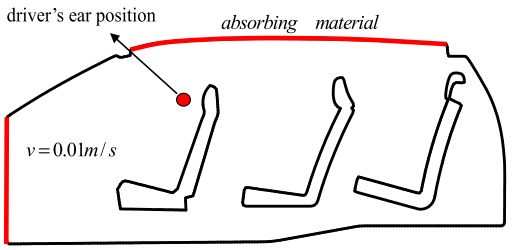

Fig. 21. Acoustic problem for a 2D MPV with different boundary conditions.

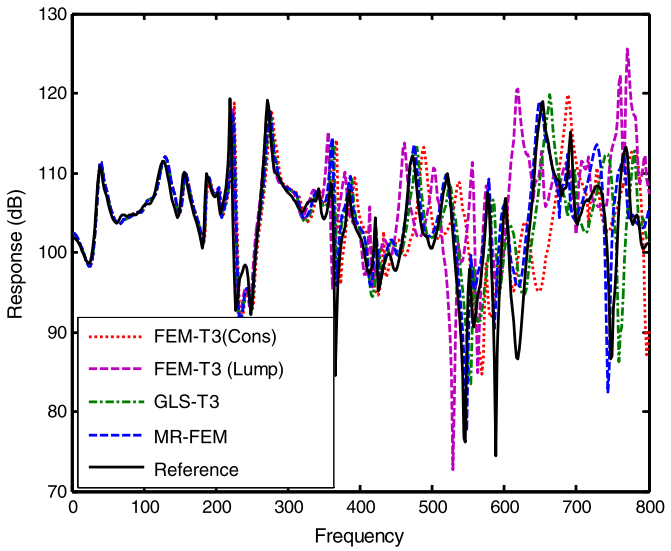

Fig. 22. Acoustic frequency response at driver's ear point for 2D MPV using MR-FEM and FEM.

(sound pressure level) at the driver's ear point obtained using FEM, GLS and MR-FEM in the 2 Hz ~ 800 Hz frequency range with a frequency resolution of 2 Hz. Because the analytical solution is unavailable for this problem, a reference configuration using FEM with a very fine mesh (10025 nodes with 19182 elements) is adopted and the result is also plotted in Fig. 22. It can be obviously observed in the figure that the deviation between FEM solutions and reference is becoming larger and larger with the increase of frequencies, and the GLS can give an improved results compared to FEM using different mass matrices. Comparing the results between the MR-FEM and GLS, it is found that the MR-FEM can provide better results than GLS in the range of studied frequencies, even the frequencies exceed 541 Hz. This practical numerical study also demonstrates that the MR-FEM can provide much more accurate frequency response analysis, even at high frequencies in real engineering problems.

6. Conclusions and discussions

In this paper, a mass-redistributed finite element method (MR-FEM) for solving acoustic problems by re-distribute the entries of the mass matrix to "tune" the balance is proposed, which is able to minimize the dispersion errors. In the present MR-FEM, the stiffness matrix is left alone, but the mass matrix of the discretization systems is modified by shifting the integration points away from the Gaussian locations, while ensuring the mass conservation. Both theoretical and numerical studies have shown that the MR-FEM works ideally for acoustic problems, and the following conclusions can be summarized:

a) The MR-FEM uses the simplest three-node triangular mesh, which can be used for generating mesh automatically for any complex domains. No pre-processing, no additional parameters,or degrees of freedoms are introduced, and the present method can be implemented in a straightforward way with little change to the FEM code.
b) It can also be found that the optimized Gauss point location for triangular mesh will lead to the mass matrix that is identical to the averaging of consistent and lumped mass matrix.
c) Among the two kinds of triangular meshes studied, the FEM, GLS and MR-FEM using hexagonal mesh can provide more accurate results than them using regular mesh. It can also be observed that the FEM (Lump) can give better results than FEM (Cons) by using regular mesh when wavenumber is relatively small; For hexagonal mesh, the FEM (Lump) always gives worse results than FEM (Cons).

d) Owing to the perfect balance of the mass matrix to the stiffness matrix in the discretized system, the MR-FEM using triangular mesh can provide great accuracy in acoustic pressure and gradient solution, much better natural eigenfrequencies prediction and higher computational efficiency than the FEM using same set of triangular mesh and even better than the FEM using quadrilateral mesh in acoustic simulation.
e) For the practical acoustic problems with complicated domains and boundary conditions, the MR-FEM provides more accurate results than the FEM and GLS in acoustic pressure spatial prediction and frequency response solution with the same set of mesh. It is indicated that the present MR-FEM has great potential in the practical analysis of acoustic problems for much more accurate solutions without additional costs.

Note that in the formulation of MR-FEM for higher order elements in 2D and 3D problems, the balance between the discretized stiffness and mass matrix is also important. The balance by introducing the symmetric permutations for the Gauss point location in calculating the stiffness and mass matrix can also be tuned, and this will be present in our next step.

Acknowledgements

The authors wish to thank the support of National Natural Science Foundation of China (Grant No. 11202074, Grant No. 61232014). It is also partially supported by the Fund of State Key Laboratory of Advanced Design and Manufacturing for Vehicle Body Nos. 31315002 and 51375001. The work by the 3rd author is supported by the United States NSF Grant under the award No. 1214188.

References

[1] F. Ihlenburg, Finite Element Analysis of Acoustic Scattering, Springer-Verlag, New York, 1998.
[2] T.W. Wu, Boundary Element in Acoustics: Fundamentals and Computer Codes, WIT Press, Southampton, 2000.
[3] F. Ihlenburg, I. Babuška, Finite element solution of the Helmholtz equation with high wave number. Part I: the h-version of the FEM, Comput. Math. Appl. 30 (9) (1995) 9–37.
[4] C.K.W. Tam, J.C. Webb, Dispersion–relation-preserving finite difference schemes for computational acoustics, J. Comput. Phys. 107 (1993) 262–281.
[5] F.Q. Hu, M.Y. Hussaini, J.L. Manthey, Low-dissipation and low-dispersion Runge–Kutta schemes for computational acoustics, J. Comput. Phys. 124 (1996) 177–191.
[6] D.W. Zing, H. Lomax, H.M. Jurgens, High-accuracy finite-difference scheme for linear wave propagation, SIAM J. Sci. Comput. 17 (1996) 328–346.
[7] R. Hixon, E. Turkel, High-accuracy compact Mc-Cormack-type schemes for computational aeroacoustics, AIAA Paper 98-0365, 1998.
[8] C.C. Stolk, A dispersion minimizing scheme for the 3-D Helmholtz equation based on ray theory, J. Comput. Phys. 314 (2016) 618–646.
[9] I. Harari, E. Turkel, Accurate finite difference methods for time-harmonic wave propagation, J. Comput. Phys. 119 (2) (1995) 252–270.
[10] G. Sutmann, Compact finite difference schemes of sixth order for the Helmholtz equation, J. Comput. Appl. Math. 203 (1) (2007) 15–31.
[11] E. Turkel, D. Gordon, R. Gordon, S. Tsynkov, Compact 2D and 3D sixth order schemes for the Helmholtz equation with variable wave number, J. Comput. Phys. 232 (1) (2013) 272–287.
[12] I. Harari, A survey of finite element methods for time-harmonic acoustics, Comput. Methods Appl. Mech. Eng. 195 (13–16) (2006) 1594–1607.
[13] L.L. Thompson, A review of finite-element methods for time-harmonic acoustics, J. Acoust. Soc. Am. 119 (2006) 1315–1330.
[14] I. Harari, T.J.R. Hughes, Galerkin/least-squares finite element methods for the reduced wave equation with nonreflecting boundary conditions in unbounded domains, Comput. Methods Appl. Mech. Eng. 98 (3) (1992) 411–454.
[15] L.L. Thompson, P.M. Pinsky, A Galerkin least-squares finite element method for the two-dimensional Helmholtz equation, Int. J. Numer. Methods Eng. 38 (1995) 371–397.
[16] I. Harari, C.L. Nogueira, Reducing dispersion of linear triangular elements for the Helmholtz equation, J. Eng. Mech. ASCE 128 (2002) 351–358.
[17] I. Babuška, F. Ihlenburg, E.T. Paik, S.A. Sauter, A generalized finite element method for solving the Helmholtz equation in two dimensions with minimal pollution, Comput. Methods Appl. Mech. Eng. 128 (3–4) (1995) 325–359.
[18] L. Franca, C. Farhat, A. Macedo, M. Lessoine, Residual-free bubbles for the Helmholtz equation, Int. J. Numer. Methods Eng. 40 (1997) 4003–4009.
[19] M. Ganesh, S.C. Hawkins, A fully discrete Galerkin method for high frequency exterior acoustic scattering in three dimensions, J. Comput. Phys. 230 (1) (2011) 104–125.
[20] L.L. Thompson, P. Kunthong, A residual based variational method for reducing dispersion error in finite element methods, in: 2005 ASME International Mechanical Engineering Congress and Exposition, November 5–11, 2005, Orlando, Florida, The American Society of Mechanical Engineers, Paper IMECE2005-80551.
[21] S. Dey, D.K. Datta, J.J. Shirron, M.S. Shephard, p-Version FEM for structural acoustics with a posteriori error estimation, Comput. Methods Appl. Mech. Eng. 195 (2006) 1946–1957.
[22] M.A. Sprague, T.L. Geers, Spectral elements and field separation for an acoustic fluid subject to cavitation, J. Comput. Phys. 184 (1) (2003) 149–162.
[23] W. Desmet, A wave based prediction technique for coupled vibro-acoustic analysis, KULeuven, division PMA, Ph.D. Thesis 98D12, 1998.
[24] B. Van Genechten, D. Vandepitte, W. Desmet, A direct hybrid finite element–wave based modelling technique for efficient coupled vibro-acoustic analysis, Comput. Methods Appl. Mech. Eng. 200 (5) (2011) 742–764.
[25] T. Belytschko, Y.Y. Lu, L. Gu, Element-free Galerkin methods, Int. J. Numer. Methods Eng. 37 (1994) 229–256.
[26] J.M. Melenk, I. Babuška, The partition of unity finite element method: basic theory and applications, Comput. Methods Appl. Mech. Eng. 139 (1–4) (1996) 289–314.
[27] G.R. Liu, Meshfree Methods: Moving Beyond the Finite Element Method, 2nd edition, CRC Press, Boca Raton, USA, 2009.
[28] O. Cessenat, B. Despres, Application of an ultra weak variational formulation of elliptic PDES to the two-dimensional Helmholtz problem, SIAM J. Numer. Anal. 35 (1) (1998) 255–299.
[29] C. Farhat, I. Harari, L.P. Franca, The discontinuous enrichment method, Comput. Methods Appl. Mech. Eng. 190 (2001) 6455–6479.
[30] N.C. Nguyen, J. Peraire, F. Reitich, et al., A phase-based hybridizable discontinuous Galerkin method for the numerical solution of the Helmholtz equation, J. Comput. Phys. 290 (2015) 318–335.
[31] C. Wenterodt, Ov. Estorff, Dispersion analysis of the meshfree radial point interpolation method for the Helmholtz equation, Int. J. Numer. Methods Eng. 77 (2009) 1670–1689.

[32] Z.C. He, G.R. Liu, Z.H. Zhong, S.C. Wu, G.Y. Zhang, A.G. Cheng, An edge-based smoothed finite element method (ES-FEM) for analyzing three-dimensional acoustic problems, Comput. Methods Appl. Mech. Eng. 199 (2009) 20–33.
[33] G.R. Liu, A generalized gradient smoothing technique and the smoothed bilinear form for Galerkin formulation of wide class of computational methods, Int. J. Comput. Methods 5 (2008) 199–236.
[34] G.R. Liu, T.T. Nguyen, Smoothed Finite Element Methods, CRC Press, Boca Raton, 2010.
[35] G.R. Liu, G.Y. Zhang, Smoothed Point Interpolation Methods: G Space Theory and Weakened Weak Forms, World Scientific, Singapore, 2013.
[36] Z.C. He, A.G. Cheng, G.R. Liu, Z.H. Zhong, G.Y. Zhang, A.G. Cheng, Dispersion free analysis of acoustic problems using the alpha finite element method, Comput. Mech. 46 (6) (2010) 867–881.
[37] Z.C. He, A.G. Cheng, Z.H. Zhong, G.Y. Zhang, G.R. Liu, Dispersion error reduction for acoustic problems using the edge-based smoothed finite element method (ES-FEM), Int. J. Numer. Methods Eng. 86 (11) (2011) 1322–1338.
[38] Z.C. He, G.Y. Li, Z.H. Zhong, A.G. Cheng, G.Y. Zhang, Eric Li, G.R. Liu, An ES-FEM for accurate analysis of 3D mid-frequency acoustics using tetrahedron mesh, Comput. Struct. 106–107 (2012) 125–134.
[39] G.R. Liu, G.Y. Zhang, Upper bound solution to elasticity problems: a unique property of the linearly conforming point interpolation method (LC-PIM), Int. J. Numer. Methods Eng. 74 (2008) 1128–1161.
[40] K.J. Marfurt, Accuracy of finite difference and finite element modeling of the scalar and elastic wave equation, Geophysics 49 (1984) 533–549.
[41] S. Krenk, Dispersion-corrected explicit integration of the wave equation, Comput. Methods Appl. Mech. Eng. 191 (2001) 975–987.
[42] G. Seriani, S.P. Oliveira, Optimal blended spectral-element operators for acoustic wave modeling, Geophysics 72 (5) (2007) 95–106.
[43] M.N. Guddati, B. Yue, Modified integration rules for reducing dispersion error in finite element methods, Comput. Methods Appl. Mech. Eng. 193 (3–5) (2004) 275–287.
[44] A. Idesman, D. Pham, Finite element modeling of linear elastodynamics problems with explicit time-integration methods and linear elements with the reduced dispersion error, Comput. Methods Appl. Mech. Eng. 271 (2014) 86–108.
[45] G.R. Liu, S.S. Quek, Finite Element Method: A Practical Course, Butterworth-Heinemann, 2003.
[46] G.R. Liu, On partitions of unity property of nodal shape functions: rigid-body-movement reproduction and mass conservation, Int. J. Comput. Methods 13 (2016) 1640003.